Analysis of optical pulse coding in spontaneous Brillouin-based distributed temperature sensors

Marcelo A. Soto*, Gabriele Bolognini, Fabrizio Di Pasquale

Scuola Superiore Sant'Anna, via G. Moruzzi 1, 56124 Pisa, Italy
**Corresponding author: m.soto@sssup.it*

Abstract: A theoretical and experimental analysis of optical pulse coding techniques applied to distributed optical fiber temperature sensors based on spontaneous Brillouin scattering using the Landau-Placzek ratio (LPR) scheme is presented, quantifying in particular the impact of Simplex coding on stimulated Brillouin and Raman power thresholds. The signal-to-noise ratio (SNR) enhancement and temperature resolution improvement provided by coding are also characterized. Experimental results confirm that, differently from Raman-based sensors, pulse coding affects the stimulated Brillouin threshold, resulting in lower optimal input power levels; these features allow one to achieve high sensing performance avoiding the use of high peak power pulses.

OCIS codes: (060.2370) Fiber optics sensors; (290.5830) Scattering, Brillouin; (120.4825) Optical time domain reflectometry.

References and links

1. "Optical-fibre Sensors," Tech. Focus Nature Photon. **2**, 143-158 (2008).
2. H. H. Kee, G. P. Lees, and T. P. Newson, "1.65 μm Raman-based distributed temperature sensor," Electron. Lett. **35**, 1869-1871 (1999).
3. M. Niklès, L. Thévenaz, and P. A. Robert, "Simple distributed fiber sensor based on Brillouin gain spectrum analysis," Opt. Lett. **21**, 758-760 (1996).
4. X. Bao, L. Zou, Q. Yu, and L.Chen, "Development and applications of the distributed temperature and strain sensors based on Brillouin scattering," *in Proceeding of IEEE Sensors Conf.* 2004, vol **3**, pp. 1210 – 1213.
5. Y. T. Cho, M. Alahbabi, M. J. Gunning, and T. P. Newson, "50-km single-ended spontaneous-Brillouin-based distributed-temperature sensor exploiting pulsed Raman amplification," Opt. Lett. **28**, pp. 1651-1653 (2003).
6. X. Bao, D. J. Webb, and D. A. Jackson, "Combined distributed temperature and strain sensor based on Brillouin loss in an optical fiber," Opt. Lett. **19**, 141-143 (1994).
7. K. Hotate and M. Tanaka, "Distributed fiber Brillouin strain sensing with 1-cm spatial resolution by correlation-cased continuous-wave technique," IEEE Photon. Technol. Lett. **14**, 197–199 (2002).
8. A. Minardo *et al.*, "A reconstruction technique for long-range stimulated Brillouin scattering distributed fibre-optic sensors: experimental results," Meas. Sci. Technol. **16**, 900-908 (2005).
9. M. A. Soto, P. K. Sahu, G. Bolognini, and F. Di Pasquale, "Brillouin-based distributed temperature sensor employing pulse coding," IEEE Sens. J. **8**, 225-226 (2008).
10. P. C. Wait and T. P. Newson, "Landau Placzek ratio applied to distributed fiber sensing," Opt. Commun. **122**, 141-146 (1996).
11. K. De. Souza *et al*, "Improvement of signal-to-noise capabilities of a distributed temperature sensor using optical preamplification," Meas. Sci. Technol. **12**, 952- 957 (2001).
12. P. C. Wait, K. De Souza, and T. P. Newson, "A theoretical comparison of spontaneous Raman and Brillouin based fibre optic distributed temperature sensors," Opt. Commun. **144**, 17-23 (1997).
13. K. De Souza and T. P. Newson, "Brillouin-based fiber-optic distributed temperature sensor with optical preamplification," Opt. Lett. **25**, 1331-1333 (2000).
14. Y. T. Cho, M. N. Alahbabi, M. J. Gunning, and T. P. Newson, "Enhanced performance of long range Brillouin intensity based temperature sensors using remote Raman amplification," Meas. Sci. Technol. **15**, 1548-1552 (2004).
15. Y. T. Cho, M. N. Alahbabi, G. Brambilla, and T. P. Newson, "Distributed Raman Amplification Combined With a Remotely Pumped EDFA Utilized to Enhance the Performance of Spontaneous Brillouin-Based Distributed Temperature Sensors," IEEE Photon. Technol. Lett. **17**, 1256-1258 (2005).

#101489 - $15.00 USD Received 12 Sep 2008; revised 17 Oct 2008; accepted 17 Oct 2008; published 4 Nov 2008

16. J. Park *et al*, "Raman-based distributed temperature sensor with Simplex coding and link optimization," IEEE Photon. Technol. Lett. **18**, 1879-1881 (2006).
17. M. Nazarathy et al., "Real-time long-range complementary correlation optical time-domain reflectometer," J. Lightwave Technol. **7**, 24-38 (1989).
18. M. D. Jones, "Using Simplex codes to improve OTDR Sensitivity," IEEE Photon. Technol. Lett. **15**, 822–824 (1993).
19. D. Lee *et al*, "Analysis and Experimental Demonstration of Simplex Coding Technique for SNR Enhancement of OTDR," *In Proceeding of IEEE LTIMC*, (New York, USA, 2004), pp. 118-122,.
20. M. Harwit and N. J. A. Sloane, *Hadamard Transform Optics* (New York: Academic, 1979).
21. G. P. Agrawal, *Nonlinear Fiber Optics*, 2nd ed. (New York: Academic, 1995).
22. R. Courant and D. Hilbert, *Methods of Mathematical Physics*, Vol. II, (Wiley New York, 1962).
23. Y. Aoki, K. Tajima, and I. Mito, "Input Power Limits of Single-Mode Optical Fibers due to Stimulated Brillouin Scattering in Optical Communication Systems," J. Lightwave Technol. **6**, 710-719 (1988).
24. K. De Souza, "Significance of coherent Rayleigh noise in fibre-optic distributed temperature sensing based on spontaneous Brillouin scattering," Meas. Sci. Technol. **17**, 1065-1069 (2006).

1. Introduction

Optical fiber sensors are recently attracting a significant interest for their many fields of applications, from industrial usage to environmental and structural monitoring [1]. Distributed fiber sensors in particular possess promising features, notably allowing continuous and spatially-resolved measurements of physical fiber parameters, such as temperature and strain, over fiber lengths of several kilometers with spatial resolutions ranging from a meter scale to a sub-cm scale, thus leading to thousands of virtually equivalent discrete sensing points. The most commonly exploited optical phenomena for deploying distributed sensors are scattering effects such as spontaneous Raman and Brillouin scattering.

Sensors based on Raman scattering offer the possibility of simpler implementation schemes (mainly due to the wide spectral separation between the pump and the Raman scattered wavelengths), but are sensitive to temperature only and are characterized by very low backscattered power levels, making the use of high peak power light sources necessary [2]. Brillouin-based distributed sensors, on the other hand, generally require more complex implementation schemes due to the small spectral separation between pump and Brillouin-scattered wavelengths [3], but are characterized by higher backscattering power values and offer the possibility of simultaneous sensing of both strain and temperature [4].

The implementations of strain and temperature Brillouin-based sensors are manifold, ranging from schemes exploiting spontaneous Brillouin scattering [5], to advanced schemes based on stimulated Brillouin scattering involving gain or loss measurements [6,7]. Such schemes, based on stimulated Brillouin scattering, generally provide higher signal-to-noise ratio (SNR) values at the receiver and are consequently characterized by a higher attainable accuracy; they can lead to cm-scale and sub-cm-scale spatial resolutions. However, they require access to both fiber ends and involve more complex implementations and processing for an accurate parameter estimation (e.g. taking into account the consideration of non-local effects [8]). On the other hand, schemes based on spontaneous Brillouin scattering, although characterized by lower sensing accuracy, require access to one fiber end only with a simpler implementation, especially in the Landau-Placzek ratio based receiver scheme [5]. We have recently presented a Brillouin-based distributed temperature sensor (BDTS) using the LPR scheme [9], where Simplex-coding was applied for SNR enhancement in the direct-detection of spontaneous Brillouin intensity up to 20 km distance, experimentally pointing out a strong influence of coding in stimulated Brillouin threshold.

In this work, we perform a thorough analysis of the benefits and issues related to optical pulse coding applied to spontaneous Brillouin-based sensors employing LPR. We detail the theoretical analysis and numerical models which are necessary to accurately describe all the arising effects in a BDTS employing pulse coding, considering in particular the impact of pulse coding on the stimulated Brillouin and Raman thresholds. Theoretical predictions are then verified by experiments, where Simplex coding is shown to allow a significant performance enhancement in a BDTS system up to a distance of 30 km. From both theory and

#101489 - $15.00 USD Received 12 Sep 2008; revised 17 Oct 2008; accepted 17 Oct 2008; published 4 Nov 2008

experiments, we conclude that the use of coding not only increases the receiver SNR with respect to single pulse case (thus leading to an improved temperature accuracy), but, at the same time, also requires lower optimum input power values, allowing for cost-effective solutions based on low-power sources, without optical pulse amplification.

This paper is organized as following: Section 2 describes the basic theory of pulse coding applied to Brillouin based distributed sensors using the Landau-Placzek ratio; in Section 3 we then present a theoretical analysis aimed at studying the impact of pulse coding in Brillouin sensors, and in particular its effect on the stimulated Brillouin threshold. In Section 4 the experimental set-up of BDTS system is presented, while experimental results are reported and discussed in Section 5. Section 6 reports the final considerations and conclusions.

2. Basic theory

2.1 Brillouin-based sensing using the Landau-Placzek ratio

Distributed temperature sensors based on Brillouin scattering can be implemented by using optical time-domain reflectometry (OTDR) technique, where an optical pulse is sent down along the sensing fiber and the Brillouin backscattered light intensity is detected. The temperature dependence of Brillouin signal intensity allows one to derive the distributed temperature profile along the sensing fiber [5]. The backscattered Rayleigh signal, which does not provide information on fiber temperature, is used as a reference signal to compensate for possible fiber loss variations. The ratio of Rayleigh scattering intensity to spontaneous Brillouin backscattered intensity, known as Landau-Placzek ratio (LPR), provides the temperature information along the sensing fiber. For a mono-component glass silica fiber, the LPR can be expressed through the well-known formula [10]:

$$\frac{I_{RS}}{I_{SpBS}} = \frac{T_f}{T}(\beta_T \rho_0 v_s^2 - 1) \tag{1}$$

where β_T is the isothermal compressibility, ρ_0 the density, T_f the fictive temperature, v_s the acoustic velocity, and $I_{RS,}$ I_{SpBS} are the intensities of Rayleigh scattering and spontaneous Brillouin scattering respectively. Note that, unlike in Raman-based distributed temperature sensors, the LPR does not require any correction factor for wavelength-dependent losses due to the small frequency separation between Rayleigh scattering and Brillouin-scattered signals (~ 11 GHz for silica fibers).

In order to reliably determine the actual temperature profile along the sensing fiber, the LPR at the unknown temperature T is typically compared with one LPR curve obtained with the fiber at a reference temperature T_R, as shown by the following equation [11]:

$$T = \frac{1}{K_T}\left(1 - \frac{LPR(T)}{LPR(T_R)}\right) + T_R \tag{2}$$

where K_T is the temperature sensitivity of the sensor.

For a correct temperature derivation, Brillouin scattering light should be limited to the spontaneous regime, with a linear dependence on the input peak power. When the peak pulse power increases above a given threshold value, fiber nonlinearities appear, resulting in a depletion of the pump pulses as well as a distortion of the Brillouin-scattered traces and hence of the temperature profile along the sensing fiber. For sensing applications this nonlinear regime is unsuitable, limiting the maximum peak pulse power to be launched into the sensing fiber. The most important nonlinearities in Brillouin sensing are stimulated Raman scattering (SRS) and stimulated Brillouin scattering (SBS), which limit the maximum usable pump power launched into the fiber below a given threshold value (P_{th}), which can be expressed by [12]:

#101489 - $15.00 USD Received 12 Sep 2008; revised 17 Oct 2008; accepted 17 Oct 2008; published 4 Nov 2008

$$P_{th} = \frac{A_{eff} C_{R,B}}{g_{R,B} L_{eff}} \tag{3}$$

where $g_{R,B}$ are the Raman and Brillouin gain coefficients, $C_{R,B}$ are dimensionless constants for Raman and Brillouin scattering respectively, A_{eff} is the fiber effective area, and L_{eff} is the effective interaction length. Note that the threshold power values for light pulses are very different in case of stimulated Raman and Brillouin scattering. In particular, for Raman scattering of pulsed light, the threshold power is dictated by the effective length considering the Raman-scattered light co-propagating with the pump [12]. The situation is different for Brillouin scattering, where the counter-propagating nature of the Brillouin components with respect to the pump leads to an effective length which is proportional to the pulsewidth. In particular, if the fiber attenuation is negligible over the fiber length L_p corresponding to one pulsewidth ($\alpha L_p << 1$), then the effective length is equal to half the pulse length ($L_{eff} = L_p/2$) [12].

Moreover, due to the large difference in the gain bandwidth for Raman and Brillouin effects (~1 THz and ~30 MHz respectively), the used source linewidth also has a significant different impact on the threshold. In fact, while the source linewidth does not have a significant impact on the threshold for the onset of SRS, a large linewidth source allows for a notably higher threshold power for onset of SBS with respect to a narrow-linewidth one.

Since the temperature accuracy in DBTS using LPR is ultimately determined by the signal-to-noise ratio (SNR) at the receiver, then, in addition to the receiver electric noise, the received optical power level is a critical parameter for the sensor performance. In OTDR-based distributed optical fiber sensors, the optical power level at the receiver is proportional to the input light pulse duration, and hence it is inversely proportional to the spatial resolution. This feature leads to a critical trade-off between spatial resolution and temperature accuracy (or equivalently sensing range). If the input pulse power is limited by the SRS or SBS threshold value, then, for a given spatial resolution, the SNR cannot be improved beyond a certain level, hence limiting the maximum temperature resolution achievable by the system at a specified sensing distance. Different techniques have been proposed to overcome this trade-off, aiming at increasing the SNR in a Brillouin intensity-based DTS. For instance, using an erbium-doped fiber amplifier (EDFA) as a preamplifier [13], or making use of distributed Raman amplification [14,15], the temperature accuracy of the sensor has been improved for long distance sensing applications.

Also, the use of optical pulse coding can overcome the trade-off between temperature or spatial resolution and the sensing distance range, as shown in [16] for Raman based distributed temperature sensors, resulting in a simple and effective solution for such applications. Thus, using optical pulse coding could in principle provide a significant SNR enhancement in BDTS systems, if compared to conventional single-pulse case, without the need of optical pulse amplification. This feature, combined with the use of simple receiver schemes, makes pulse coding applied to BDTS an attractive technology.

Note however that the simplified expression for the effective length ($L_{eff} = L_p/2$) cannot unfortunately be used in case of pulse coding, especially for long codewords. This is because the basic assumptions required to obtain this expression for L_{eff} are not valid anymore with pulse coding. In that case the effective length and Brillouin threshold power must be directly derived from time-space propagation equations, as it will be shown in detail in Section 3.

2.2 Optical coding techniques in sensing applications

For sensing applications based on direct detection schemes, only aperiodic and unipolar pulse codes can be used, similarly to OTDR systems. Coding schemes can be classified into two general groups: correlation codes and linear combination codes.

Within the first group, a suitable correlation scheme which has been successfully used in OTDR, and recently applied also to optical fiber sensors, is based on the complementary-correlation Golay codes [17]. They are based on code pairs characterized by good correlation

#101489 - $15.00 USD Received 12 Sep 2008; revised 17 Oct 2008; accepted 17 Oct 2008; published 4 Nov 2008

properties. In that scheme, sets of optical pulses are launched down the sensing fiber depending on the different codewords. To obtain the decoded trace, backscattered signals are then correlated with the corresponding transmitted codes, obtaining the impulse backscattering fiber response. Due to the high required dynamic range, mainly in long distance sensing applications, the used codes should have low side-lobes not to create ghost peaks in the temperature trace due to intensity variations in other fiber locations.

Within the second group, a coding scheme which has been shown to be particularly efficient in optical fiber sensing applications is based on Simplex coding [18,19]. This is not envisaged as a correlation coding, but it rather involves linear combinations of traces following the so-called S-matrix [18]. The S-matrix is an unipolar version of a modified Hadamard matrix; rows of this matrix are orthogonal and can be easily generated using quadratic residues methods, shift-register sequences and twin primes [18]. Simplex coding is performed by modulating the intensity of an optical source according to the codewords given by the row vectors of this unipolar S-matrix. Decoding is performed by simple linear matrix algebra with the measured coded traces obtained from different codewords. Within the class of codes employing linear algebra transformations, the Simplex coding scheme is particularly efficient, as mentioned above, for improving the sensor performance, since it can be demonstrated that Simplex coding is *A*-optimal [20] within its class for a given code length. This means that the root mean square (*rms*) noise at the receiver is minimized when using Simplex coding, allowing for the best achievable performance.

The SNR enhancement provided by coding is quantified by the coding gain G_{COD}, defined as the ratio of the SNR obtained (at a given fiber distance) when using pulse coding with respect to the SNR obtained with single pulses (for the same number of total acquired traces to provide a fair comparison). For Simplex coding, the coding gain G_{COD} for an arbitrary code length L_c, considering a zero-mean uncorrelated noise and a large receiver bandwidth, is given by [19]:

$$G_{cod} = \frac{L_c + 1}{2\sqrt{L_c}} \tag{4}$$

The effectiveness of the SNR enhancement provided by Simplex-coding has been demonstrated for applications such as OTDR systems [18,19] and Raman-based distributed temperature sensors [16]. In such cases, pulse coding has led to performance improvement and to accurate temperature measurements, for a given spatial resolution, with a negligible influence on degrading nonlinear effects (such as stimulated Raman scattering). However, due to the different physical properties of Brillouin scattering with respect to Raman scattering, the effectiveness of coding for spontaneous Brillouin-based sensor is not straightforward. For instance, the narrower gain bandwidth, the counter-propagating direction of scattering light and the required use of narrowband sources in case of Brillouin-based sensors can greatly reduce the threshold for onset of stimulated Brillouin scattering. Actually, as it will be detailed in Section 3, the pulse coding process significantly decreases the power threshold for onset of stimulated Brillouin scattering, an effect which has never been observed in Raman-based sensing.

3. Effective length of coded signals and SBS threshold calculation

Unfortunately, in order to accurately calculate the effective length in case of BDTS systems using coded optical pulses, the simple expression for L_{eff} reported in Section 2 cannot be used. In fact, for long codewords (e.g. 127 bit or higher) the spatial extent of the optical coded pulses within the fiber becomes large, and the fiber absorption effect cannot be neglected. In this case, the solution of the time-space model of Brillouin scattering is required, leading to a set of differential equations describing the interaction between electric fields and acoustic waves [21]. In a quasi-CW regime (i.e. the optical intensities and the nonlinear phase temporal changes are considered slow compared to the photon lifetime $\tau_B = 1/\Gamma_B$), the dynamics of the acoustic wave can be neglected [21]. Under these assumptions, the evolution of optical

#101489 - $15.00 USD Received 12 Sep 2008; revised 17 Oct 2008; accepted 17 Oct 2008; published 4 Nov 2008

intensities over time, t, and space, z, for the forward-propagating pump light $I_P(z,t)$ and backward-propagating Stokes Brillouin light $I_B(z,t)$ can be described by the following equations [21]:

$$\frac{\partial I_P}{\partial z}+\frac{n}{c}\frac{\partial I_P}{\partial t}=-g_B I_P I_B-\alpha I_P \tag{5}$$

$$\frac{\partial I_B}{\partial z}-\frac{n}{c}\frac{\partial I_B}{\partial t}=-g_B I_P I_B+\alpha I_B \tag{6}$$

where n is the effective index of the fiber mode, c is the speed of light in the vacuum, g_B is the Brillouin gain coefficient, and α is the fiber attenuation coefficient (considered as identical at pump and Stokes Brillouin wavelengths).

The boundary conditions for the system of equations given by Eqs. (5)-(6) are:

$$I_P\left(z=0,t\right)=I_{Po}\left(t\right),\qquad I_B\left[z=z_L\left(t\right),t\right]=I_{Bo}\left(t\right) \tag{7}$$

where $I_{Po}(t)$ represents the time dependence of the pump pulses at the fiber input, and $I_{Bo}(t)$ represents the spontaneous Brillouin intensity at a distance $z_L(t)$ from which SBS is originated. Note that the boundary condition for $I_B(z,t)$ in Eq. (7) represents the occurrence of SBS from the initial spontaneous Brillouin scattering generated in a small section of the fiber near the rear edge of the pulse at distance $z_L(t)$, which depends on the position of the pump pulse at a given time t.

In order to find a semi-analytical solution of the system of equations (5)-(6) we can use the characteristic method [22], which allows us to find a general solution of the system in time, t, and distance, z. In such a method, the solution of the system of equations is found through suitable changes of variables and integration over a given z-t subspace defined by the characteristic curves (i.e. coordinate transformation systems, which in our case consist essentially in two reference frames moving along opposite directions along the optical fiber with the speed of light). The characteristic curves suitable for the solution of the system (5)-(6), defining the new variables χ_P and χ_B, result to be:

$$\Gamma_1:\chi_P=t-\frac{n}{c}z \tag{8}$$

$$\Gamma_2:\chi_B=t+\frac{n}{c}z. \tag{9}$$

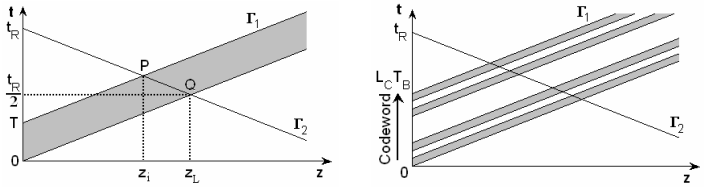

Fig. 1. Characteristic t-z curves defined by Eqs. (8)-(9) employed in the solution of the system of Eqs. (5)-(6). (a) Single-pulse case. (b) Coded-pulses case.

Figure 1 gives a schematic representation of the characteristic curves. While Γ_1 refers to the case of an input square pulse of time duration T (Fig. 1a) as well as to the case of coded pulses (Fig. 1b) with a codeword duration L_cT_B (L_c bits within a codeword with bit duration T_B), the curves Γ_2 in Fig. 1 are related to the corresponding backward-propagating reference frame arriving at $t=T_R$ at the fiber input.

#101489 - $15.00 USD Received 12 Sep 2008; revised 17 Oct 2008; accepted 17 Oct 2008; published 4 Nov 2008

Therefore, in Fig. 1, the first set of characteristic curves (Γ_1) physically represents the evolution of pump pulses along the fiber, while the second set of characteristics (Γ_2) describes the backward propagation evolution of the Brillouin light scattered from different fiber locations with the same arrival time t_R at the fiber input.

Considering that the pump depletion due to spontaneous Brillouin scattering can be considered negligible, then the evolution of the pump power $I_P(z,t)$ in Eq. (5) can be simply found through integration over the Γ_1 characteristic curve, giving:

$$I_P(z,t) = I_{Po}\left(t - \frac{n}{c}z\right)\exp(-\alpha z) \tag{10}$$

To obtain the Brillouin backscattered signal at the fiber input as a function of time $I_B(z=0,t)$, then Eq. (6) must be solved by integration over the Γ_2 characteristic curve frame. In case of input light pulses with a finite temporal duration, this integration can be expressed with a semi-analytical expression:

$$I_B(z=0,t) = I_{Bo}\left(\frac{t}{2}\right)\exp\left[-\alpha\left(\frac{c}{2n}t\right) + g_B\int_{z_i(t)}^{z_L(t)} I_P\left(\xi, t-\frac{n}{c}\xi\right)d\xi\right] \tag{11}$$

where $I_P(\xi,t-n\xi/c)$ is given by Eq. (10). Note that the integration is performed only from $z_i(t)$ to $z_L(t)$, positions which define the interaction length of the optical waves as represented in Fig. 1a. This length of fiber corresponds to half the pulse duration ($\Delta z \equiv z_L - z_i = cT/2n$), because the two fields do not interact along the characteristic curve Γ_2 when they are not spatially overlapping (i.e. at times $t < t_R/2$ and $t > t_R/2+T/2$).

In the case of single pulses with a finite time duration, the integral boundaries $z_i(t)$ and $z_L(t)$, for a given time t, can then be expressed as [22]:

$$z_i(t) = \frac{c}{2n}(t-T), \qquad z_L(t) = \frac{c}{2n}t \tag{12}$$

allowing one to calculate the Brillouin power at the fiber input from Eq. (11).

When pulse coding is applied, in order to obtain a semi-analytical solution of Eq. (11), the corresponding integral must be calculated in all the space-time regions where the Brillouin backscattered light is superimposed with the forward-propagating pulses within each codeword. Unfortunately in such a condition it is not possible to find one a single general analytical expression for all codewords, since such an expression would depend of the specific position of '1' and '0' bits within each codeword.

Nevertheless, in order to calculate the power threshold, we can assume a worst-case condition which is given by the situation where the Brillouin backscattered power reaching the fiber input at a given time t is maximum. In case of Simplex coding scheme, this worst-case scenario essentially consists in considering an input codeword where all the '1' pulses are adjacent, thus producing a longer continuous optical pulse (such a worst-case codeword is indeed defined within the S-matrix and has a number of adjacent '1' bits equal to $(L_c+1)/2$).

For the worst-case condition, it is sensible to calculate the extent of Brillouin backscattered power where the effects of fiber attenuation are minimum, i.e. near the fiber input. Therefore, the Brillouin backscattered power should be evaluated at a time t corresponding to the overall duration of the adjacent optical pulses generated within the worst-case codeword mentioned above. Under this condition, we can then infer that the highest Brillouin backscattered signal at the fiber input for the worst-case codeword occurs at $t_{MAX} = T_B(L_c+1)/2$, where T_B is the bit duration. Thus, the integral in Eq. (11) can be calculated as:

$$\int_{z_i=0}^{z_L'} I_P\left(\xi, t_{MAX} - \frac{n}{c}\xi\right)d\xi = I_{Po}\int_{z_i=0}^{z_L'}\exp(-\alpha\xi)\,d\xi = \frac{I_{Po}}{\alpha}\left[1-\exp(-\alpha z_L')\right] \tag{13}$$

#101489 - $15.00 USD Received 12 Sep 2008; revised 17 Oct 2008; accepted 17 Oct 2008; published 4 Nov 2008

where I_{Po} is the input peak pulse intensity and z'_L is the maximum interaction length given by

$$z'_L = \frac{c}{2n}\frac{T_B\left(L_c+1\right)}{2} \tag{14}$$

The maximum Brillouin-backscattered power reaching the fiber input is then obtained from Eqs. (11)-(14), and results to be:

$$I_B\left(z=0,t_{MAX}\right) = I_{Bo}\left(t_{MAX}/2\right)\exp\left(-\alpha z'_L + g_B I_{Po} L_{eff}\right) \tag{15}$$

where the effective length L_{eff} is given by:

$$L_{eff} = \frac{1}{\alpha}\left[1-\exp\left(\frac{-\alpha L_p\left(L_c+1\right)}{4}\right)\right] \tag{16}$$

and L_p ($=c\cdot T_B/n$) is the single bit length in a codeword.

Note that, the commonly used expression for the effective length reported in Section 2 is a specific case of Eq. (16) which is more general and also valid in case of pulse coding where the effects of fiber attenuation on the transmitted pulses cannot be neglected. For single pulse schemes (L_c = 1) where the fiber attenuation is negligible ($\alpha L_p/2 << 1$) due to the short used pulse duration, the effective length in Eq. (16) is reduced to $L_p/2$, which corresponds to the well-known expression for OTDR and conventional-BDTS [12].

Figure 2 reports the Brillouin threshold power, as well as a comparison of SBS and SRS thresholds, computed according to Eq. (3) and Eq. (16), as a function of the code length for different spatial resolution values. For threshold calculation, typical parameter values of dispersion-shifted fibers have been used ($g_R = 10^{-13}$ m^{-1}, $g_B = 5\text{x}10^{-11}$ m^{-1}, α = 0.25 dB/km, $\Delta\lambda_{Raman}$ = 113 nm [12]). We can clearly see that the Brillouin threshold, which is a function of the pulse width, decreases significantly with the use of Simplex coding, because of the increment in the effective interaction length. On the other hand, the co-pumping nature of stimulated Raman scattering results in a different effect when coding is applied.

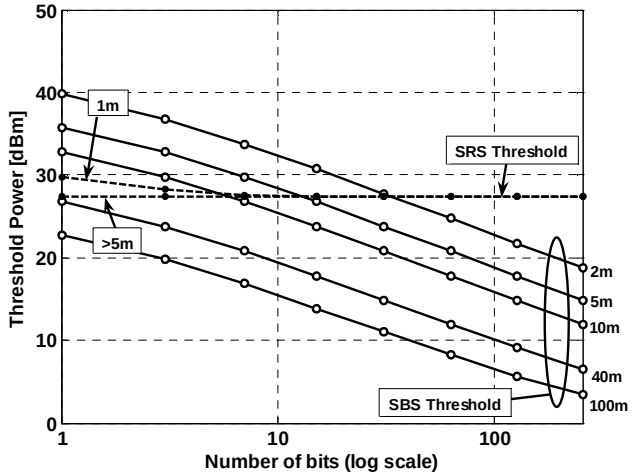

Fig. 2. Threshold power for both SRS (dotted line) and SBS (solid line) versus number of bits within a codeword, for different spatial resolution settings.

According to Fig. 2, when the code length is less than 7 bit and pulses are shorter than 50 ns, the effective length for Raman scattering is dominated by the walk-off distance. This produces an effective length which is mainly proportional to the pulse width, hence, being affected by the code length used for coding. However, for longer pulses (> 50 ns) the effective

#101489 - $15.00 USD Received 12 Sep 2008; revised 17 Oct 2008; accepted 17 Oct 2008; published 4 Nov 2008

length is dominated by the fiber attenuation, being independent of the pulse width, producing a Raman threshold tending towards a constant value. When longer code lengths are used (≥ 15 bit), the effective length becomes dominated by the fiber attenuation, producing a constant SRS threshold independently of the code length and spatial resolution used by the sensor.

Actually, in case of single-pulsed BDTS, the effective length results to be independent of the fiber attenuation, due to the short duration of the pulse [12]. However, when coding is applied, the length used by the codewords into the sensing fiber must be taken into account. For example, a 255-bit Simplex codeword, with a spatial resolution of 10 m, has a considerable length of ~5.1 km along the fiber, so that the effect of fiber attenuation cannot be neglected in such case.

Unlike single-pulsed DTS, where the limiting nonlinear effect depends of the pulse width (SRS limits the system for short pulses, while SBS for longer pulses [12]), in case of coded BDTS, the limiting factor is given by the onset of SBS in most practical conditions (e.g. considering codes longer than 32 bits for coding gain G_{COD} > 4.58 dB, and spatial resolution ≥ 2 m). However, for code length < 32 bit, the limiting effect can be either SBS or SRS, depending of the spatial resolution as shown in Fig. 2.

For efficient increment of SBS threshold, the spectrum of the optical source must be broadened above the SBS linewidth (~30 MHz). This can be done by laser current dithering, providing a power threshold given by [23]

$$P_{th} = \frac{A_{eff} C_{R,B}}{g_{R,B} L_{eff}} \left(\frac{\Delta\nu_B + \Delta\nu_p}{\Delta\nu_B} \right) \tag{17}$$

where $\Delta\nu_p$ is the effective linewidth of the laser, and $\Delta\nu_B$ is the SBS gain linewidth. Therefore, SBS thresholds shown in Fig. 2 may be increased as described in Eq. (17). Laser dithering inducing a broadening in the effective linewidth of the laser also allows for a reduction of coherent Rayleigh noise (CRN) in Rayleigh trace used in LPR [24]. However, the effective linewidth of the laser should be narrower than 11 GHz to avoid overlapping of Rayleigh and Brillouin components, thus limiting the CRN reduction.

Other techniques can be used in Rayleigh measurements in order to further reduce the impact of CRN. They will be described more in detail in the next section.

4. Experimental setup for Simplex coded-BDTS

Figure 3 shows the experimental set-up used to study spontaneous Brillouin-based DTS employing Simplex-coding. The used light source is a tunable external cavity laser (ECL) with a linewidth of 200 kHz and operating at 1550.0 nm. The CW-light is amplified by an EDFA and optically filtered by a tunable bandpass filter (OF, 0.8 nm FWHM) to reduce the amplified spontaneous emission (ASE) noise. A polarization-controller (PC) is introduced at the input of a Mach-Zehnder modulator (MZI) which is driven by a waveform generator (WFG), providing single pulses as well as 127-bit Simplex-coded pulses.

The pulse duration is 400 ns, corresponding to about 40 m spatial resolution. In order to allow temperature measurement in single-pulsed DBTS at peak pulse power levels higher than the SBS threshold, the EDFA and the optical filter (OF) can be moved after the MZI (not shown in Fig. 3). Note that, when the EDFA is placed after the MZI, pulse coding cannot be used because the slow transient of the EDFA would distort the codewords, affecting the effectiveness of this technique. Light pulses are then coupled into the sensing fiber, through a three-port optical circulator, which is composed of three spools (10.5 km, 1 km, and 18.5 km) of dispersion-shifted fiber (DSF) for a total length of 30 km. First and third fiber spools have been kept at room temperature (300 K), while the temperature of the midway fiber spool (1 km length) has been changed during experiments by placing it inside a temperature-controlled chamber (TCC), which allows for an accurate control of the fiber temperature.

#101489 - $15.00 USD Received 12 Sep 2008; revised 17 Oct 2008; accepted 17 Oct 2008; published 4 Nov 2008

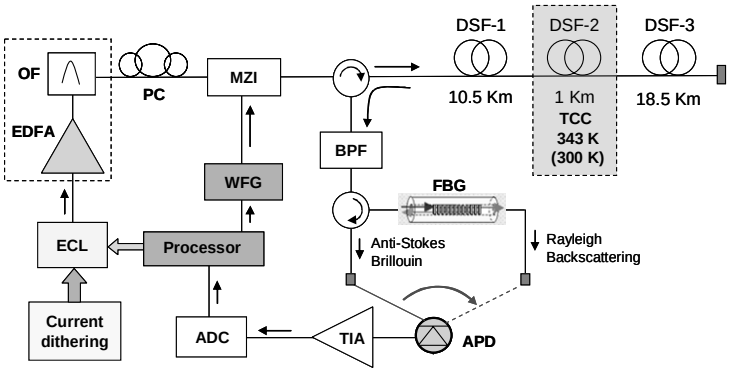

Fig. 3. Experimental set-up of the implemented sensor system.

In order to increase the power threshold value before the onset of detrimental stimulated Brillouin scattering, current dithering has been applied to the laser source to broaden its linewidth. This also helps in reducing CRN in the Rayleigh trace measurement. Temporal amplitude fluctuations produced by CRN on the backscattered Rayleigh signal can be further reduced by sweeping the optical frequency of the laser and averaging a large number of independent backscattered Rayleigh traces [24]. By reasonably assuming an average number large enough to reduce the noise of the receiver below CRN, a similar state of polarization for the pump and the backscattered Rayleigh signal, and scattering elements of the order of the pump wavelength, the standard deviation of the CRN normalized to the Rayleigh intensity is given by [24]:

$$f_{CRN} = \sqrt{\frac{V_g}{4\Delta z \Delta f}} \tag{18}$$

where V_g is the group velocity, Δz is the spatial resolution of the sensor and Δf is the sweeping band of the laser.

Note that for Brillouin-based DTS systems, wavelength averaging is needed only for Rayleigh measurements, because spontaneous Brillouin scattering is not affected by coherent fading noise due to the random phase variations induced in the photon-photon scattering process [24].

Hence, in order to further reduce the CRN, we have also applied a wavelength-averaging technique by sweeping the frequency of ECL over 60 GHz (in this scheme, the acquisition of the Rayleigh trace is time-interleaved with the anti-Stokes Brillouin trace acquisition). This helps reducing the impact of CRN down to 0.4%, i.e. negligible with respect to the power noise in Rayleigh trace near fiber input.

The receiver block for detecting the light backscattered from the sensing fiber is based on a low-loss direct-detection scheme. This is composed of a three-port optical circulator combined to a narrowband fiber Bragg grating (FBG, 6 GHz bandwidth at anti-Stokes port), and a detection stage given by a high gain InGaAs avalanche photodiode (APD, 80 MHz) followed by a high gain transimpedance amplifier (TIA) and by an analog-digital converter (ADC). The narrowband FBG (spectral characteristics are reported in Fig. 4) is used to separate the anti-Stokes Brillouin-scattered light (reflected component in the FBG) from the Rayleigh-scattered light (pass signal in the FBG) into two different circulator ports, with a high band rejection (28 dB).

#101489 - $15.00 USD Received 12 Sep 2008; revised 17 Oct 2008; accepted 17 Oct 2008; published 4 Nov 2008

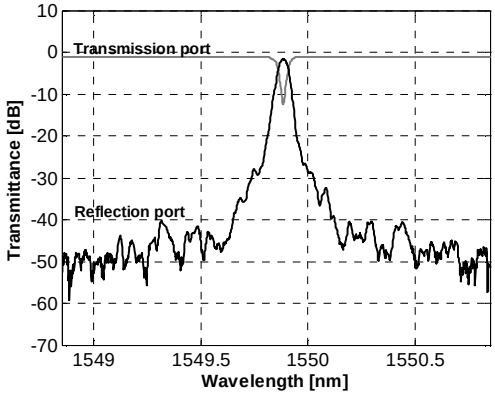

Fig. 4. Transmission and reflection spectra of the narrowband FBG.

5. Results

5.1 Temperature measurements

The temperature estimation along the sensing fiber has been obtained by measuring Rayleigh and anti-Stokes Brillouin scattering light through the setup of Fig. 3, and using Eq. (2), taking the room temperature (300 K) as a reference. Measurements have been carried out by using both single pulses and pulse coding according to Simplex coding scheme. In both cases, 180000 total traces were acquired and averaged, allowing for an attainable acquisition time, similar in both cases, of the order of 1 min, excluding processing overhead.

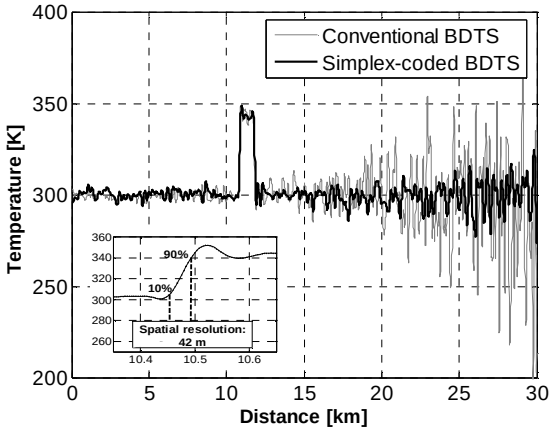

Fig. 5. Temperature distribution along the fiber (TCC at 343 K) for single pulses BDTS (gray line) and 127-bit Simplex-coded BDTS (black line). Inset, spatial resolution achieved by Simplex-coded and single-pulse BDTS.

Figure 5 shows the calculated temperature distribution along the sensing fiber when the fiber inside the TCC is at 343 K and the input peak power of the pump light is 10 dBm. We can clearly see that the temperature accuracy achieved using coded-BDTS is better than the one obtained with the conventional single-pulse scheme, due to the SNR enhancement provided by the 127-bit Simplex coding (~7 dB). The inset in Fig. 5 shows the measured spatial resolution achieved by the BDTS, which was found to be 42 m (estimated as the 10% to 90% response distance), a value which was nearly identical for single pulse and coded case.

#101489 - $15.00 USD Received 12 Sep 2008; revised 17 Oct 2008; accepted 17 Oct 2008; published 4 Nov 2008

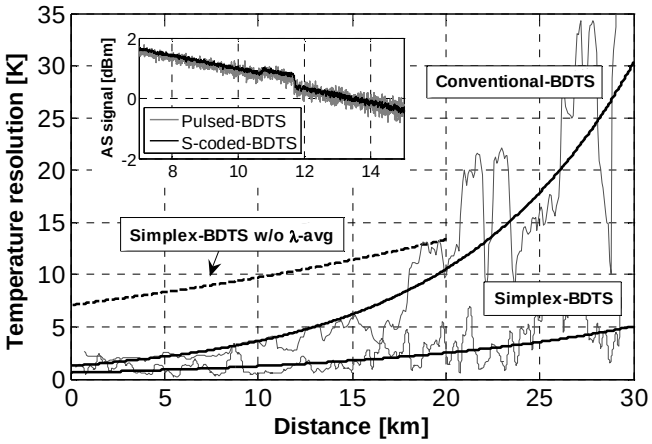

Fig. 6. Temperature resolution as function of fiber length, for conventional-BDTS, and 127-bit Simplex coded BDTS with and without λ-averaging.

In the inset of Fig. 6, which reports the acquired anti-Stokes traces with and without coding, we can clearly see the achieved SNR enhancement when Simplex-coding is used. The SNR improvement measured near the fiber end (7.1 dB) is in good agreement with the theoretical expectation from Eq. (4), predicting 7.5 dB improvement. Such a SNR enhancement has a strong beneficial impact on the attained temperature resolution, calculated by fitting the *rms* of the difference between the estimated and the real temperatures, as shown in Fig. 6. For the single-pulse case the achieved temperature resolution is ~30 K near fiber end (30 km distance), and it is enhanced down to 5.0 K with the use of 127-bit Simplex coding.

At fiber input, for both single-pulsed and Simplex-coded BDTS, the temperature resolution results to be ~1 K. This is related to CRN from the Rayleigh trace in the LPR of Eq. (2). Its impact results to be more evident near the fiber input due to the combined effects of: *i)* stronger CRN near fiber input due to a shorter related path length, and *ii)* better SNR values in the anti-Stokes trace near fiber input. Figure 6 also shows the impact of CRN on the temperature resolution. In the first 20 km of the sensing fiber, the BDTS scheme without wavelength averaging (dotted lines) would provide a worse temperature resolution than BDTS with λ-averaging, especially near fiber input. Temperature resolutions are better in single-pulse and Simplex case when using λ-averaging, since the limitation arises from the CRN in the Rayleigh trace.

The reduction of CRN was achieved by sweeping the optical frequency of the laser source over 60 GHz (0.5 nm in the range 1549.95 – 1550.43 nm) every 2 pm. Thus, 240 separate backscatter traces have been measured and then averaged, allowing for a reduction of phase correlation between backscattered lightwaves. In Fig. 7, the CRN measured without frequency sweeping is compared with the one obtained when sweeping, and subsequent λ-averaging over 0.5 nm, is applied. The corresponding fluctuations (lower than 0.4%) reflect a significant reduction of CRN in the Rayleigh traces. The experimental CRN provided by frequency sweeping agrees with the theoretical estimation obtained from Eq. (18) (predicting CRN = 0.45%).

Note that wavelength averaging is not required in the anti-Stokes Brillouin measurements because they are not affected by CRN due to the random phase fluctuations associated with spontaneous Brillouin scattering. Therefore, no frequency sweeping is applied to the optical frequency of the laser during anti-Stokes Brillouin measurements, allowing us to use the narrowband FBG (reported in Fig. 4) to separate anti-Stokes Brillouin component from Rayleigh signal.

#101489 - $15.00 USD Received 12 Sep 2008; revised 17 Oct 2008; accepted 17 Oct 2008; published 4 Nov 2008

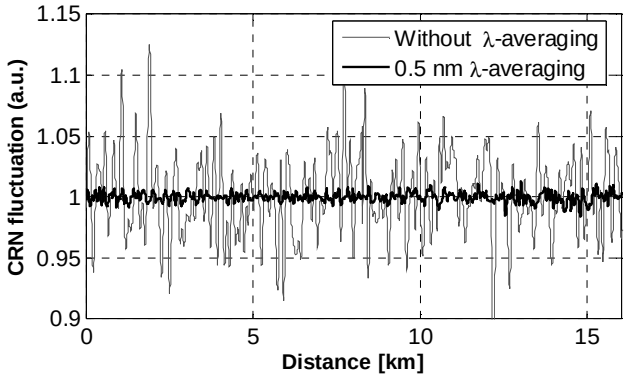

Fig. 7. Coherent Rayleigh noise fluctuations versus distance obtained with (black line) and without (gray line) λ-averaging.

5.2 Impact of stimulated Brillouin scattering threshold

Figure 8 shows the measured temperature (at 4 km distance from fiber input) versus input pulse peak power, for conventional and Simplex-coded BDTS, when all the sensing fiber is kept at room temperature (300 K). The figure also shows the measurement error range, given by the rms noise in temperature trace. The maximum error range between measured temperature (from data of Fig. 8) and real temperature is summarized in Table 1. It can be seen that the uncertainty in temperature measurement is reduced (and consequently the accuracy is improved) for higher input power levels, until occurrence of nonlinear effects (i.e. mainly SBS) which induce an unpredictable deviation of measured temperature from real temperature value (such a deviation is mainly due to SBS-induced depletion in Anti-Stokes trace).

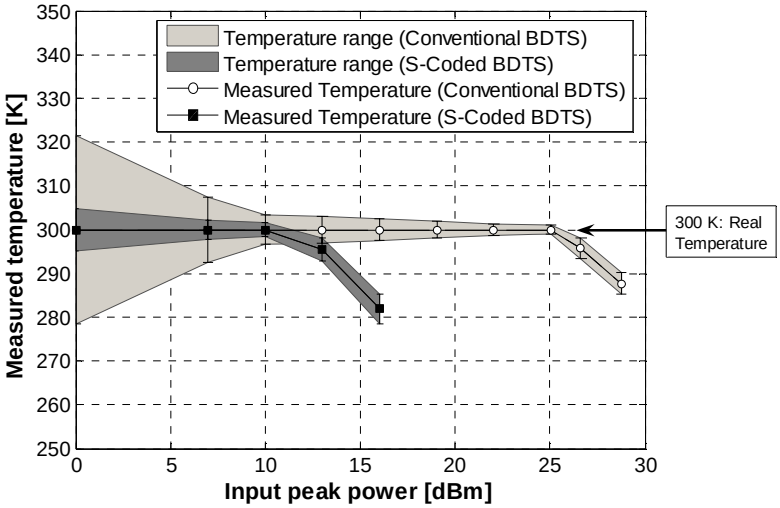

Fig. 8. Measured temperature and error range (standard deviation) at 4 km distance versus input peak power for 127-bit Simplex-coded BDTS (squares) and conventional-BDTS (circles).

From Fig. 8 and Table 1, it is clear that the highest usable input power threshold value P_{th}, before the onset of nonlinear effects, is strongly affected by the use of coding, as correctly predicted by theory. Actually, the SBS threshold power with single-pulsed BDTS is about 25 dBm, while with Simplex-coding P_{th} is about 10 dBm. This is occurring since the coding process leads to a longer pulse effective length (at the same spatial resolution) with respect to

#101489 - $15.00 USD Received 12 Sep 2008; revised 17 Oct 2008; accepted 17 Oct 2008; published 4 Nov 2008

single pulses. Therefore Simplex-BDTS allows one to achieve the optimum at an input peak power which is ~15 dB lower than in case of conventional-BDTS, allowing one to avoid optical pulse amplification. Thus, SBS threshold can limit the ability of pulse coding to achieve an overall better temperature resolution with respect to the single pulse case; such a drawback is not present in distributed Raman temperature sensors, where this effect has never been observed for practical code lengths.

Table 1. Maximum temperature error in measurements at 4 km distance

Input Power [dBm]	Temperature error [K]	
	S-Coded BDTS	*Conventional BDTS*
0.0	4.7	21.6
7.0	2.1	7.6
10.0	1.5	3.3
13.0	4.5	3.1
16.0	18.1	2.5
19.0	--	1.8
22.0	--	1.4
25.0	--	1.3
26.6	--	4.2
28.8	--	12.4

Actually, Fig. 9 reports the temperature distribution along the sensing fiber (at room temperature) obtained using single-pulse BDTS as well as the distribution obtained using coded-BDTS, when the input peak power is 16 dBm in both cases (note that this value is higher than the SBS threshold for 127-bit Simplex coded-BDTS). When employing Simplex coding, we can see from Fig. 9 that stimulated Brillouin scattering produces a clear distortion in the measured temperature trace, causing an error of ~18 K (at 4 km distance) in the temperature estimation due to depletion in anti-Stokes trace.

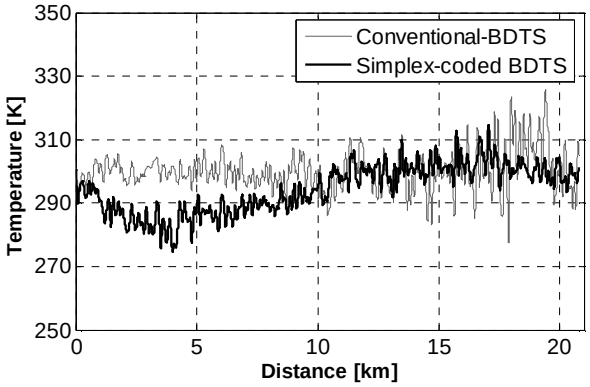

Fig. 9. Temperature distribution along the sensing fiber, with input P_{peak} = 16 dBm, for conventional (gray line) and Simplex-coded (black line) BDTS.

6. Conclusions

In conclusion, an analysis of the impact of optical pulse coding techniques on BDTS based on LPR has been carried out. An enhanced performance in BDTS has been demonstrated using optical pulse coding. Experimental results have shown that 127-bit Simplex coding provides

#101489 - $15.00 USD Received 12 Sep 2008; revised 17 Oct 2008; accepted 17 Oct 2008; published 4 Nov 2008

7.1 dB SNR improvement, allowing for 30 km sensing range with a temperature accuracy better than 5.0 K and spatial resolution equal to 42 m, using only 10 dBm pulse peak power at the fiber input. The theoretical study has pointed out a strong impact of pulse coding in reducing stimulated Brillouin threshold power. Experimental results have also confirmed that pulse coding reduces the power threshold for the onset of stimulated Brillouin scattering, allowing for an optimum temperature resolution, which is similar to single-pulse case at sensibly lower input peak power. Coding techniques can then be successfully applied as an alternative to optical amplification in BDTS systems, providing a high-performance cost-effective solution when high power pulses cannot be employed.

#101489 - $15.00 USD Received 12 Sep 2008; revised 17 Oct 2008; accepted 17 Oct 2008; published 4 Nov 2008